JOURNAL OF GEOPHYSICAL RESEARCH, VOL. 112, D18110, doi:10.1029/2007JD008645, 2007

Chemical behavior of the tropopause observed during the Stratosphere-Troposphere Analyses of Regional Transport experiment

L. L. Pan,[1] K. P. Bowman,[2] M. Shapiro,[3,4] W. J. Randel,[1] R. S. Gao,[5] T. Campos,[1] C. Davis,[1] S. Schauffler,[1] B. A. Ridley,[1] J. C. Wei,[6] and C. Barnet[7]

Received 9 March 2007; revised 24 May 2007; accepted 27 June 2007; published 26 September 2007.

[1] During the Stratosphere-Troposphere Analyses of Regional Transport (START) experiment in December 2005, the behavior of the extratropical tropopause was examined under a variety of dynamical conditions. Using in situ measurements of ozone and water vapor, on board the new NSF/NCAR research aircraft Gulfstream V, and data from large-scale meteorological analyses, we address issues of the tropopause definitions and sharpness. Comparisons of the data from two flights show that the sharpness of chemical transitions across the tropopause varies with the sharpness of the static stability change across the tropopause. Using tracer correlations, air masses of mixed stratospheric and tropospheric characteristics are identified. The mixed air mass does not form a uniform mixing layer near the tropopause, but rather shows strong spatial variation. A depth of mixed air (~5 km in vertical distribution) is found on the cyclonic side of the polar jet, where the thermal gradient is weak and significant separation occurs between the thermal and the dynamical tropopause. Away from the jet or on the anticyclonic side of the jet, where the stability gradient is strong, the chemical transition across the tropopause was much more abrupt and shows minimum mixing. In both cases (either significant or minimal mixing), the thermal tropopause is shown to be approximately at the center of the mixing layer, and the altitude relative to the thermal tropopause is found to be an effective coordinate for locating the chemical transition. To further understand the role of the thermal and dynamical tropopause as a chemical transport boundary, tracer correlations are used to examine the chemical characteristics, and the trajectory calculations are used to infer the fate of the air mass between the thermal and dynamic tropopauses in the region of significant separation. The tracer correlation analysis shows that the air mass in this region is a mixture of stratospheric and tropospheric air but predominantly of tropospheric characteristics. Trajectory model calculations show that a significant fraction of the air parcels in this region ended in the mid to lower troposphere, which suggest the irreversible nature of the observed stratospheric intrusion.

Citation: Pan, L. L., et al. (2007), Chemical behavior of the tropopause observed during the Stratosphere-Troposphere Analyses of Regional Transport experiment, *J. Geophys. Res.*, *112*, D18110, doi:10.1029/2007JD008645.

1. Introduction

[2] The tropopause, defined as the upper boundary of the troposphere or "turning sphere," is a concept devised after the discovery of the stratosphere [e.g., *Hoinka*, 1997]. Definitions of the tropopause have evolved over time, depending on the questions of interest, combined with increasing observational capabilities. As a boundary surface between distinct tropospheric and stratospheric air masses, the tropopause is often considered to be a transport barrier, across which material transport is inhibited to some degree. Motivated by the need of explaining the observed chemical composition in the upper troposphere and lower stratosphere (UTLS), especially the distribution of water vapor and ozone, and the need of predicting stratosphere-troposphere exchange (STE) in a changing climate, the concept of the tropopause as a transport boundary has been revisited in recent years. A particular set of questions of interest is related to the relationship of the thermal and dynamic tropopause. The thermal tropopause, defined using the temperature lapse rate [*World Meteorological Organization* (*WMO*), 1957], considers the change of static stability as the key indicator of the transition from troposphere to stratosphere. The dynamic tropopause, defined

[1]National Center for Atmospheric Research, Boulder, Colorado, USA.
[2]Department of Atmospheric Sciences, Texas A&M University, College Station, Texas, USA.
[3]Office of Weather and Air Quality, NOAA, Boulder, Colorado, USA.
[4]Also at National Center for Atmospheric Research, Boulder, Colorado, USA.
[5]Chemical Sciences Division, Earth System Research Laboratory, NOAA, Boulder, Colorado, USA.
[6]QSS Group, Inc., Lanham, Maryland, USA.
[7]National Environmental Satellite Data and Information Service, NOAA, Camp Springs, Maryland, USA.

0148-0227/07/2007JD008645$09.00

using isentropic potential vorticity (PV), aims to locate a continuous surface that separates the chemically distinct stratospheric and tropospheric air masses [e.g., *Danielsen*, 1968; *Shapiro*, 1980; *Holton et al.*, 1995]. It is well known that the two definitions often produce different tropopause height [e.g., *Hoerling et al.*, 1991], especially in the region near jet streams where the thermal tropopause often has multiple levels and discontinuities [e.g., *Kochanski*,1955; *Palmén and Newton*, 1969; *Randel et al.*, 2007].

[3] There is also a question whether the tropopause is better characterized as a surface or a layer. In the tropics, it is now generally conceived to be more useful to consider a transition *layer*, referred to as the tropical tropopause layer or TTL, that controls upward transport into the stratosphere [*Highwood and Hoskins*, 1998; *Sherwood and Dessler*, 2000]. In the extratropics, a concept of an Extratropical Transition Layer (ExTL) has also been put forward [*WMO*, 2002; *Law et al.*, 2005]. In this work, we focus on the issue of transport boundary in the extratropics. We examine the behavior of the extratropical tropopause (ExTP) using recent research aircraft in situ data and large-scale analyses with a focus on understanding the meaning of the tropopause when the thermal and PV tropopauses do not coincide. The result is also relevant to the question of whether the ExTP should be viewed as a layer or a surface.

[4] This work is a follow-up to two types of studies. The first type consists of analyses of the tropopause, including the relationship between various definitions, particularly the thermal and PV definitions. It has long been recognized that the thermal and PV tropopause behave differently in regions of cyclonic flow, often resulting in a lower PV tropopause [e.g., *Hoskins et al.*, 1985; *Hoerling et al.*, 1991; *Wirth*, 2001]. In addition, analyses of temperature profiles from radiosondes show that the thermal tropopause is often indefinite in cyclonic regions; that is, the transition from the tropospheric static stability to the stratospheric ones occurs gradually over a larger vertical range [*Price and Vaughan*, 1993]. Furthermore, a study using ozonesonde data showed that if a tropopause definition is devised from ozone profiles, considering both the magnitude of the ozone concentration and its vertical gradient, the analyzed ozone tropopause is often below the thermal tropopause but mostly when the latter is indefinite [*Bethan et al.*, 1996].

[5] The second type of study deals with the mixing of chemical tracers near the tropopause using tracer correlations. Tracer correlation analysis is a widely used method, especially for in situ aircraft observations of the UTLS region [e.g., *Hintsa et al.*, 1998; *Marcy et al.*, 2004; *Ridley et al.*, 2004; *Hegglin et al.*, 2006]. Measurements with high spatial resolution in the extratropical UTLS region appear to show persistent mixing between stratospheric and tropospheric air near the tropopause, as indicated by the correlations of long-lived chemical tracers [*Fischer et al.*, 2000; *Zahn et al.*, 2000; *Hoor et al.*, 2002]. Using a PV tropopause definition of 2 pvu (1 pvu = 10^{-6} K m^2 kg^{-1} s^{-1}), a mixing layer can be identified above the tropopause [*Fischer et al.*, 2000; *Zahn and Brenninkmeijer*, 2003; *Hoor et al.*, 2004]. If the thermal tropopause is used, the mixing layer appears to be approximately centered at the tropopause, with a latitude-dependent depth [*Pan et al.*, 2004].

[6] In this work, we examine the mixing of chemical tracers near the tropopause in more detail and look for relationships between the mixing behavior and the thermal gradient of the tropopause region using aircraft measurements from a recent experiment. The rapid increase in static stability at the tropopause is the main cause for the tropopause to behave like a transport barrier. We expect to see that the mixing behavior near the tropopause correlates with the sharpness of the tropopause; that is, the sharpness of the chemical transition varies with the sharpness of the thermal transition across the tropopause. In particular, we seek to make connections between several previous studies to examine if the region of cyclonic flow, which is known to have a less distinctive thermal transition in the tropopause region and tends to have significant differences between the thermally defined and the PV based tropopause, is associated with a deeper chemical transition layer.

[7] The in situ observations were made on board the new US National Science Foundation (NSF) research aircraft, a Gulfstream V (GV), known as the High-performance Instrumented Airborne Platform for Environmental Research (HIAPER). Prior to the commencement of regular science missions, a series of flights were carried out with a simple instrument payload to test and demonstrate the research capability of the aircraft. These flights were designated as the Progressive Science missions (ProgSci). The Stratosphere-Troposphere Analyses of Regional Transport (START) experiment was one of the four projects conducted during the ProgSci. Five of the 13 ProgSci flights were conducted for the START experiment.

[8] The goal of the START experiment was to investigate stratosphere-troposphere exchange and the impact of dynamics on the chemical composition of the midlatitude UTLS. A small suite of chemical tracer instruments, ozone (O_3), water vapor (H_2O) and carbon monoxide (CO) were deployed together with standard meteorological sensors. With limited instrument payload, the START experiment targeted specific transport pathways and the chemical characteristics of the tropopause. The results from two selected flights are presented in this work to address the issues of the tropopause behavior. In addition to this work, these flights provided evidence of new particle formation near the tropopause fold [*Young et al.*, 2007] and a case study of UTLS chemical distribution influenced by the large-scale quasi-horizontal flow [*Bowman et al.*, 2007].

[9] In addition to the in situ measurements, the flight planning and data analyses used large-scale meteorological fields based on operational meteorological analysis from the National Centers for Environmental Prediction (NCEP) data sets. The experiment also combines aircraft measurements with global satellite data. The aircraft data are used to examine the details of the tropopause region and the satellite data are used to examine the spatial scale of the targeted events. Trajectory calculations are used to examine the origins and fate of the air mass sampled during a stratospheric intrusion.

2. Measurements and Data

2.1. In Situ Tracer Measurements

[10] During the ProgSci flights, in situ chemical tracer measurements included ozone (O_3), carbon monoxide (CO), and water vapor (H_2O). The CO instrument began to perform properly toward the end of the mission, so data are not available for many early flights. For this reason, only O_3 and H_2O data are used for the analyses in this work.

[11] In situ O_3 was measured using the NOAA Earth System Research Laboratory (ESRL) dual-beam UV-absorption ozone photometer with an overall uncertainty of ±5% and precision of 1.5×10^{10} molecules/cm^3 [*Proffitt and McLaughlin*, 1983]. The sampling rate is fixed at 1 Hz. The true time resolution of the O_3 instrument was about 2–3 s for the HIAPER configuration because of a long sample line. A number of START profiles took place in close vicinity to NOAA ESRL ozonesondes. These coordinated profile observations showed agreement to well within their stated uncertainties.

[12] In situ H_2O concentrations were measured using a MayComm Open-Path Laser Hygrometer (OPLH) sensor. This inlet-free, dual-channel instrument detects optical absorption of water vapor at 1.37 μm. Conversions from concentration/number density to mixing ratio units are achieved using fuselage mounted static pressure and air temperature sensors. H_2O is quantified with an estimated accuracy of 5–10% at a time resolution of 20 samples/s. The data used in the analyses was a binned average at 1 s sampling rate. The sensor was designed with two optical paths, 10 cm and 130 cm, to allow quantification in both high- and low-humidity environments. Information from the two channels are combined to report a single water vapor mixing ratio that is valid over a range from 1 to 30,000 ppmv. The limiting factor in assigning uncertainty is the 5% calibration system uncertainty. Comparison between the laser hygrometer and chilled mirror sensors (standard NCAR Research Aviation Facility tropospheric reference hygrometer) showed good agreement over the overlapping performance range.

2.2. Global Meteorological Analyses Data

[13] The global meteorological analyses used for flight operations and postmission analyses are from National Centers for Environmental Prediction (NCEP). Two slightly different data sets are used: the Global Forecast System (GFS) operational analysis and the Final Global Data Assimilation System (FNL) data. Both data sets are products of the NCEP global operational forecast system. The GFS use observations for 2 hours and 45 min past the analysis time to create a global analysis, which is then used to make 16-day forecasts 4 times per day. The FNL analysis uses data collected up to 6 hours past the analysis time to create a post hoc global analysis 4 times per day. The analysis and forecast system is run at the highest resolution, currently T254 L64. Analyses are provided on a $1^\circ \times 1^\circ$ global grid with 26 pressure levels from 1000 to 10 hPa. More information on the data sets can be found online at http://wwwt.emc.ncep.noaa.gov/gmb/para/parabout.html. For the applications in this work, the differences between the two data sets are negligible. For simplicity, we refer to both as GFS data in the rest of this paper.

2.3. Satellite Data

[14] Three-dimensional O_3 fields from the Atmospheric Infrared Sounder (AIRS) on the NASA Aqua satellite were used in near real time to provide a large-scale background for the GV flights. The AIRS instrument is a 2378 channel nadir cross-track scanning infrared spectrometer with a 15 km field of view (FOV) [*Fetzer et al.*, 2006]. The instrument is designed to provide high-resolution atmospheric temperature and water vapor profiles for improving weather forecasts. A number of trace gas species are also retrieved. Here, we use the Level 2 ozone profile standard product from the Version 4 retrieval algorithm [*Susskind et al.*, 2006]. The granular data are given in 45 km pixels and 28 layers. Initial validation studies have shown that the AIRS ozone profiles in the extratropical UTLS region are in good agreement with ozonesonde data. The agreement in the northern hemisphere UTLS is within 40%. Compared to ozonesondes, the AIRS ozone retrieval tend to have a high bias in the UT and a low bias in the LS, but the dynamical variability is consistent with the ozonesondes [*Bian et al.*, 2007; *Monahan et al.*, 2007]. We have also made comparisons using in situ ozone from START flights. The results will be presented elsewhere (L. Pan et al., manuscript in preparation, 2007).

2.4. ProgSci Flights 1 and 5

[15] Flight 1 took place on 1 December 2005. Tropopause folding was expected, according to the forecast, along a jet streak across the central U.S. (roughly from South Dakota to Tennessee where the subtropical, polar and Arctic jets merged) in the region of the large gradient of PV shown in Figure 1. The main research legs were chosen to be between Garden City, Kansas (37.55°N, 100.44°W) and Duluth, Minnesota (46.48°N, 92.10°W). The selected flight path was not in the area of the strongest folding as judged from the GFS analysis but in the proximity of the aircraft base (near Boulder) for more flight time to sample the vertical structure. Also shown in Figure 1 is the AIRS ozone field at 300 hPa. The ozone map shows that the jet streak marks the boundary between stratospheric and tropospheric air at 300 hPa, identified by the large gradient in ozone along the flight track.

[16] In contrast to the contorted structure of the tropopause region sampled on flight 1, flight 5, which took place on 9 December, sampled the tropopause in locations of relatively flat PV surfaces. As indicated in Figure 2, the flight took place between the main branch of the jet stream and a cutoff low near the west coast of North America. The flight path was designed to sample the region near the hyperbolic point associated with the cutoff low. The case is discussed in detail in a companion paper [*Bowman et al.*, 2007]. The AIRS ozone at the 300 hPa level is also given in Figure 2, indicating the large-scale background chemical distribution. Horizontal gradients of ozone were generally small in the region of the flight. As indicated in Figure 2, the region of flight was in a ridge, between an extended trough (east of the flight track) and the cutoff low.

[17] Figure 3 shows the flight pattern of flight 1 together with the 2 pvu surface, based on NCEP GFS 1800 UT analyses, and provides a 3-D view of the GV track and the tropopause fold sampled. To sample the structured tropopause, flight 1 was conducted in a stacked flight pattern that includes six different levels, and sampled the air mass on both sides of the jet streak and in and out of the stratospheric intrusion. The horizontal legs at multiple levels provided transects across the tropopause fold. Three vertical soundings were made around the jet (including both the cyclonic and anticyclonic side) and across the jet core, providing contrasting observations of dynamical conditions over a vertical range of $3 \sim 14$ km. During the last segment of the flight the aircraft reached the 47 kft level (380 K isentropic surface, the lower boundary of the "overworld" [*Hoskins*, 1991]).

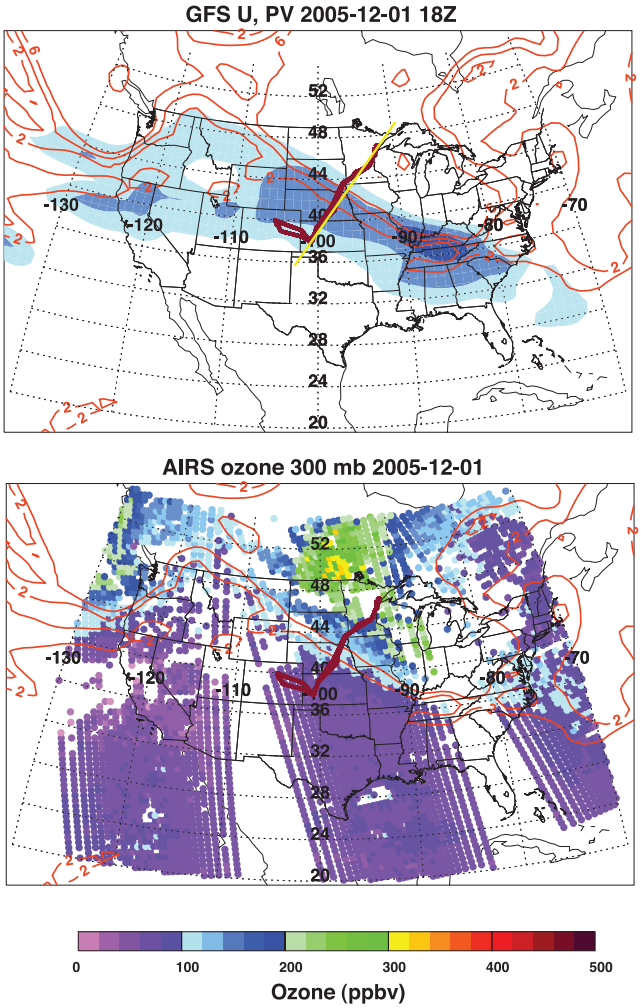

Figure 1. Synoptic-scale background for flight 1. (top) Horizontal wind (30, 40, 50 m/s, blue shadings) and PV field (2, 4, 6 pvu, orange contours) at the 300 hPa level from the NCEP GFS analyses. (bottom) AIRS ozone for the 300–250 hPa layer from the AIRS ascending data (color image) and the PV in orange contours. The ground track of the GV is marked by the dark red line in both panels. The yellow line in Figure 1 (top) marks the location of the approximate flight cross section used in analyses, which is shown in Figures 5 and 8.

[18] During flight 5, two loops were flown around a roughly triangular flight path at approximately the 300 and 250 hPa levels (projection of the flight track is shown later in Figure 5). The anchor points of the triangle were located at Cheyenne, WY (41°12.7′N, 104°46.4′W), Fairfield, UT (40°16.5′N, 111°56.4′W), and Needles, CA (34°46.0′N, 114°28.4′W). Three soundings were planned but the tropospheric portion of the sounding was not carried out at the Fairfield end because of the air traffic near Salt Lake City.

3. Analyses and Results

[19] Flights 1 and 5 were selected because the dynamical conditions sampled by the two flights provide a good contrast. Flight 1 observed a stratospheric intrusion around a jet streak, a region similar to where significant mixing has been observed in previous studies [e.g., *Shapiro*, 1980; *Cooper et al.*, 2004; *Pan et al.*, 2006]. Flight 5 was away from the jet and sampled a relatively "flat" tropopause. We begin by examining the sharpness of the chemical transition under different dynamical conditions. Trace gas profiles and tracer-tracer relationship between ozone and water vapor are then used to identify the location and the depth of the chemical transition layer. We further focus on the air mass between the thermal and the dynamical tropopause. The chemical characteristics of these air parcels provide physical insight into the meaning of the tropopause when the two definitions give different tropopause heights. Last, we use a trajectory-model calculation to examine the origin and the fate of the air masses sampled in the region of the fold to

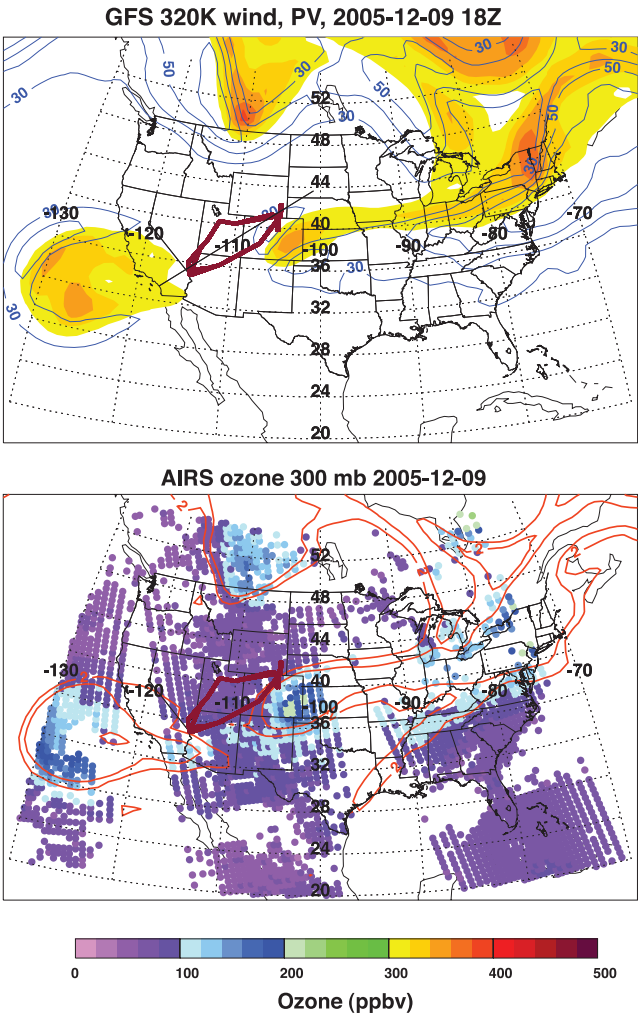

Figure 2. Synoptic-scale background for flight 5. (top) NCEP GFS PV (2,4, 6 pvu in yellow/orange shading) and the horizontal wind field (30–50 m/s in blue contours) on the 320 K theta surface. (bottom) Ozone for the 300–250 hPa layer from AIRS (color image) and PV field (2 and 4 pvu, orange contours). The ground track of the GV is marked by the dark red line in both panels. The thin black line in Figure 2 (top) marks the location of the approximate flight cross section used in analyses, which is shown in Figures 5 and 8.

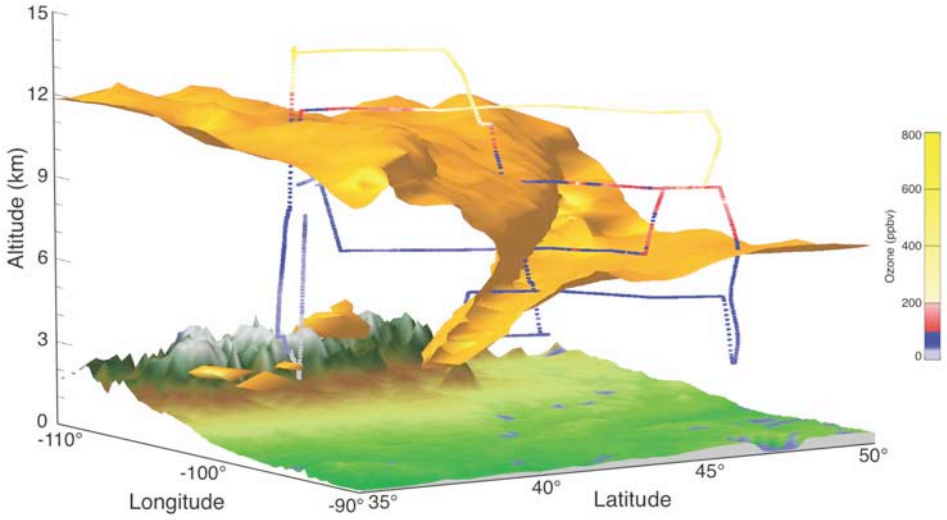

Figure 3. GV flight track for flight 1, 1 December 2005. The 2 pvu surface (orange), based on NCEP/GFS analyses at 1800 UT, indicates the spatial structure of a tropopause fold sampled by the GV. Colors on the flight track indicate the in situ ozone value from measurements on board the GV.

confirm the irreversibility of the observed intrusion, and to further understand the role of the thermal and dynamical tropopause as a transport boundary.

[20] Note that both the thermal and dynamical tropopause used in this section are from the GFS analyses (section 2.2), interpolated spatially and temporally to the flight track. We have made comparisons of these GFS interpolated thermal tropopause heights with that from the in situ temperature measurements on locations where the GV transected the tropopause. The agreement typically is within 0.5 km with the analyzed tropopause being typically lower than the GV tropopause.

3.1. Chemical Discontinuity Across the Tropopause

[21] Analyses of ozone measurements from the two flights are presented in this section to examine changes in the chemical characteristics across the tropopause. It is well known that the troposphere and stratosphere air masses are chemically distinct. In terms of ozone and water vapor, the stratosphere is ozone rich and dry, while the troposphere is ozone poor and moist. The vertical profiles of ozone and water vapor are important indicators of the tropopause location. The manner of the change (abrupt versus gradual) provides information of the sharpness of the tropopause. We expect a discontinuity in chemical tracer profiles near the tropopause and will use this property to evaluation the thermal and dynamical definitions of the tropopause, as well as the vertical coordinates suitable for displaying the chemical transition across the tropopause.

[22] Figure 4 displays ozone profiles measured during flights 1 and 5 in three different vertical coordinates. They are pressure-altitude (z), pressure-altitude relative to the analyzed thermal tropopause (z_r), and PV. At each point along the flight track the thermal tropopause altitude and PV values are interpolated from the NCEP GFS data. In the z coordinates (Figures 4a and 4d), profiles are given in two colors to separate the measurements above (red) and below (green) the thermal tropopause. Three observations can be made from Figure 4. First, the difference in the background dynamical conditions is highlighted by the profiles in z coordinates. During flight 1, the thermal tropopause altitude, indicated by the boundary between the red and the green points, varies from ~12 km on the equatorward side of the jet to ~7 km on the poleward side of the jet (see also Figure 5). The range of tropopause heights along the track of flight 5, on the other hand, is quite small (11–12 km). Second, comparisons of the profiles in z_r coordinates (Figures 4b and 4e) show that the ozone distribution changes abruptly at the tropopause in the case of a flat tropopause, and there is a near first-order discontinuity at the tropopause. The change of ozone across the tropopause in flight 1 is more gradual. Third, the profiles in PV coordinates do not show a sharp change of ozone at any particular PV value, which reflects the fact that PV and ozone are both tracers of stratospheric air masses and they correlate in the tropopause region. Figure 4 shows that typical stratospheric ozone values (100 ppbv or greater) occur at PV higher than 4 pvu.

[23] The profiles in Figure 4 lead to the conclusion that the relative altitude z_r is a better coordinate for examining the chemical transition from the troposphere to stratosphere. This result is similar to the ER-2 data analyses presented by *Pan et al.* [2004], where the chemical transition in trace gas profiles was more compact by using z_r. Figure 4 also indicates that the chemical transitions are occurring with different gradients under different conditions. To find whether this is related to the difference in thermal and dynamical background, we show in Figure 5 cross sections of static stability (given in potential temperature (θ) lapse rate, $d\theta/dz$) for the two flights from the GFS analyses, along with additional meteorological variables. Note that these cross sections are based on 1800 UT analyses for each flight day and should be viewed as an approximation, since the research flight were of roughly 8-hour duration. For flight 1, the cross section is closely aligned with the flight track spatially (Figure 1). For flight 5 we selected a cross section

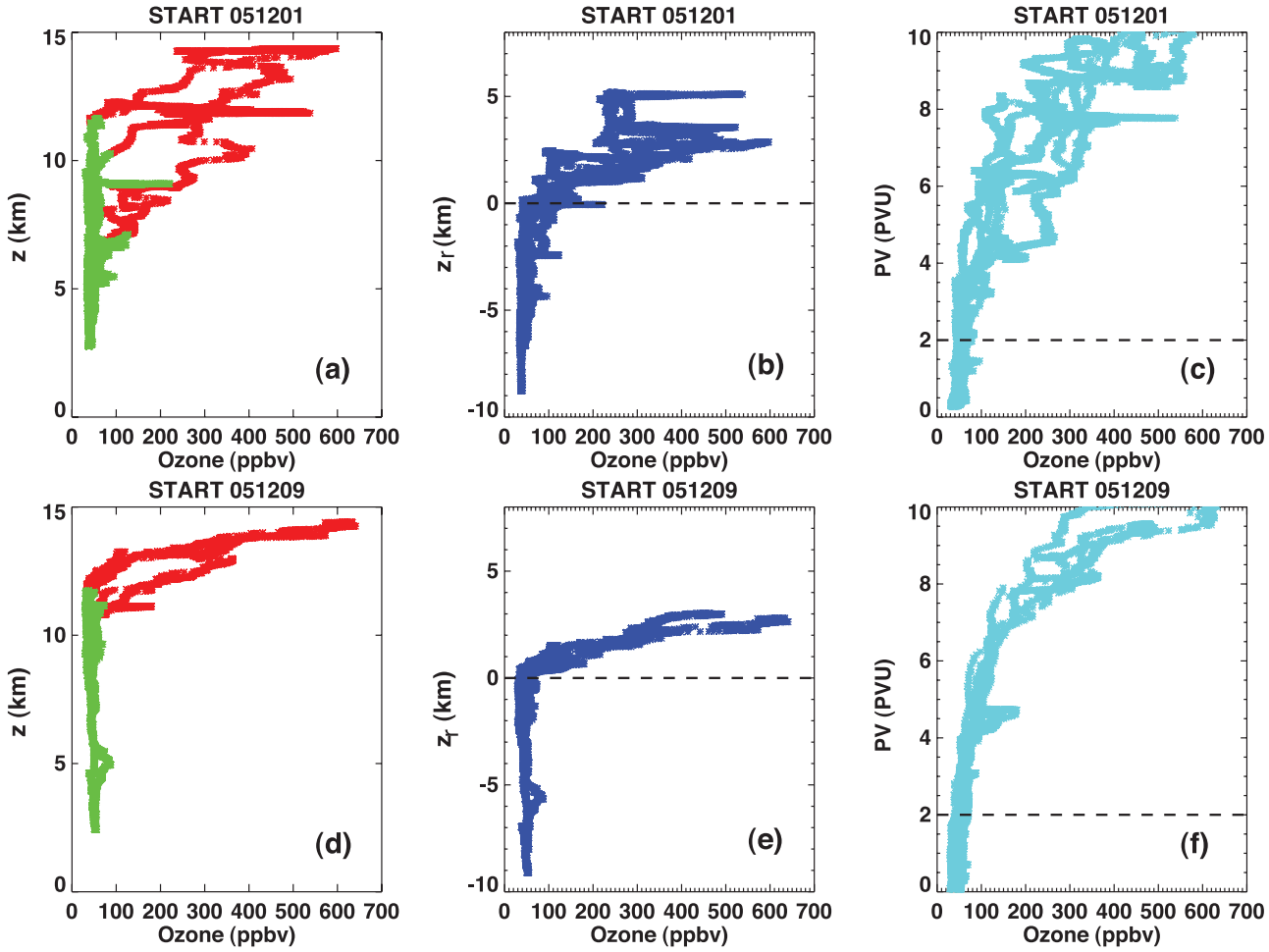

Figure 4. Ozone profiles measured on (a–c) flight 1 and (d–e) flight 5 in three sets of coordinates: pressure altitude (z), pressure altitude relative to the thermal tropopause altitude (z_r), and PV. For the profile in pressure altitude (z) (Figures 4a and 4d), the measurements are separated according to whether they are above (red) or below (green) the thermal tropopause.

approximately parallel to the long side of the triangular flight track, not directly coincident with that flight leg but representative of the region of flight (Figure 2).

[24] The layer we focus on is where the θ lapse rate is between 6 and 15 K km^{-1} (blue and green colors). This is the transition zone from tropospheric to stratospheric static stability. Part of this layer, roughly between 6–10 K km^{-1}, is similar to the range of the temperature (T) lapse rate (dT/dz) previously used to define the sharpness of tropopause from radiosondes [*Price and Vaughan*, 1993; *Bethan et al.*, 1996]. In that work, the tropopause was considered sharp or definite if the layer of T lapse rate changed from 6 K/km (characteristic of upper troposphere) to 2 K/km (base of the WMO tropopause) was less than 0.5 km, and indefinite if the layer was thicker than 1.2 km. In this work, the GFS data we use have a much coarser vertical resolution and are inappropriate for quantitative analyses in subkilometer vertical scales. We inspect this layer qualitatively to note that this layer is generally ~1–2 km, with the exception of the frontal zone in Figure 5a, where this layer shows a fold structure and expands to a much broader vertical range in this region. Together, Figure 5a shows strong contrast between the cyclonic (poleward) and anticyclonic (equatorward) side of the jet in the static stability gradient. The sharp gradient on the anticyclonic side suggests that the tropopause there forms a strong transport barrier. The much weaker gradient on the cyclonic side suggests that the tropopause in this region is less definite. The abrupt change in thermal tropopause height near 44 N shows the location of the tropopause break. This is also the region where the thermal and dynamical tropopauses (using 2 pvu surface) are significantly different; that is, the weakly defined thermal tropopause does not coincide in any simple way with any particular PV isopleth.

[25] The ozone profiles (Figure 4, in z_r coordinates) show clear correlations between the sharpness of the thermal and the chemical transitions. A sharp chemical transition is found in flight 5 and the data for the anticyclonic side of the flight 1 (not shown but is similar to the flight 5 result), where ozone mixing ratios increase at the rate of 100–150 ppbv/km right above the tropopause. In contrast, the data from the cyclonic side of the jet measured on flight 1 show ~50 ppbv/km ozone mixing ratio gradient near the tropopause. This is further examined using tracer correlations in the following section.

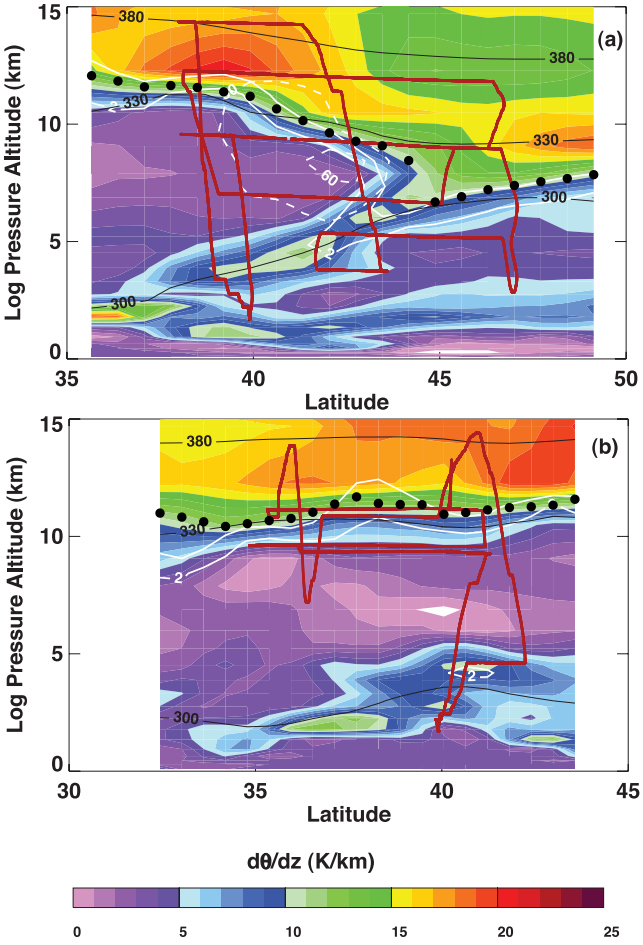

Figure 5. Static stability (color image, given in potential temperature lapse rate) of the approximate flight cross section for (a) flight 1 and (b) flight 5 in latitudinal projection. Other fields displayed are PV (white solid contours) zonal wind (white dash contours), isentropes (black lines) and the thermal tropopause (black dots). The flight tracks are shown in dark red. The map locations of the cross sections are given in Figures 1 and 2.

3.2. Chemical Transition in the Tracer-Tracer Space

[26] In this section, we examine the chemical transition and the relationship between the thermal and dynamical tropopause using a pair of stratospheric and tropospheric tracers. The most frequently used parameters for this type of study are O_3 and CO [*Fischer et al.*, 2000; *Zahn and Brenninkmeijer*, 2003; *Hoor et al.*, 2002, 2004; *Pan et al.*, 2004, 2006], because both tracers have strong gradients across the ExTP, and their chemical lifetimes are longer than the transport timescale in this region. Here, O_3 and H_2O vapor are used. Note that H_2O is not a perfect long-lived tracer in this region, because it is not conserved if air parcels encounter temperatures low enough for phase transitions. It is nevertheless an excellent tropospheric tracer with a strong gradient across the tropopause and a long history in STE studies across the ExTP [e.g., *Dessler et al.*, 1995; *Pan et al.*, 1997; *Hintsa et al.*, 1998; *Ray et al.*, 1999]. O_3-H_2O correlations have shown to be effective in identifying mixing of stratospheric and tropospheric air near the tropopause region [e.g., *Patmore and Toumi*, 2006; *Karpechko et al.*, 2007; *Pan et al.*, 2007].

[27] Figure 6 shows the O_3-H_2O correlation for flight 1, with axes scaled to emphasize the tropopause region. Two color schemes are used to display the same data. Figure 6 (top) highlights the position of the thermal tropopause, while Figure 6 (bottom) highlights the air mass *between* the thermal tropopause and the 2 pvu surface. The chemical transition between the stratosphere and troposphere forms an "L" shape in the tracer-tracer space, with a stratospheric branch and a tropospheric branch. This result is very similar to the O_3-H_2O correlation from the measurements on board the NASA ER-2 research aircraft [*Pan et al.*, 2007]. This L-shaped tracer correlation is the natural consequence of the strong gradients of the tracers across the tropopause.

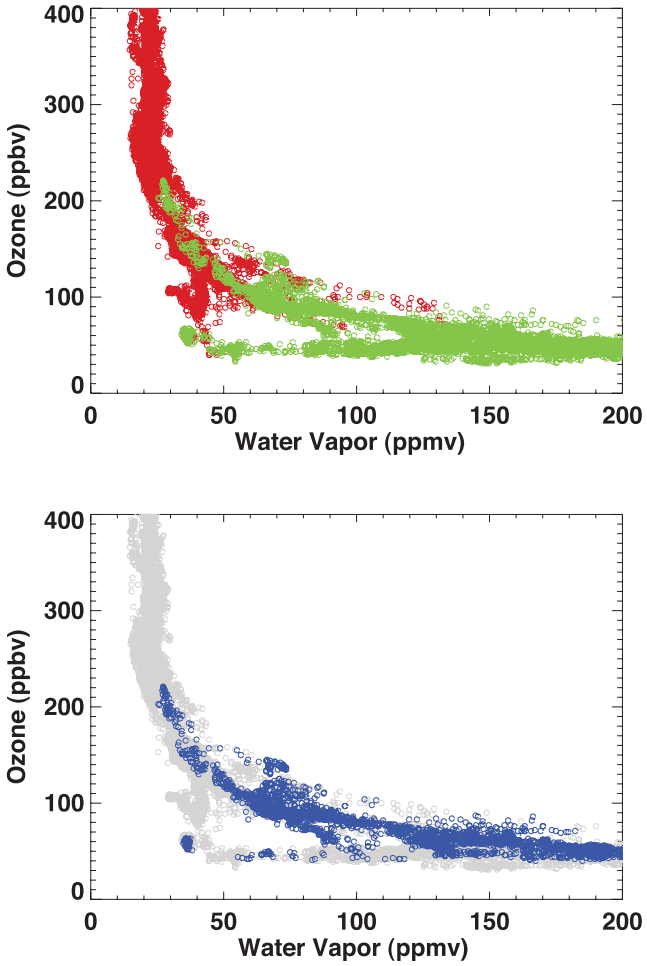

Figure 6. Correlation of ozone and water vapor measured during flight 1, with a range selection to focus on the stratosphere-troposphere transition region. The colors are used to identify the location of the thermal and dynamical tropopause in the tracer-tracer space. (top) Focuses on the thermal tropopause and the measurements above (red) and below (green) the thermal tropopause are highlighted. (bottom) Focuses on the dynamical tropopause (2 pvu surface). The measurements made between the thermal tropopause and the dynamical tropopause are highlighted (blue).

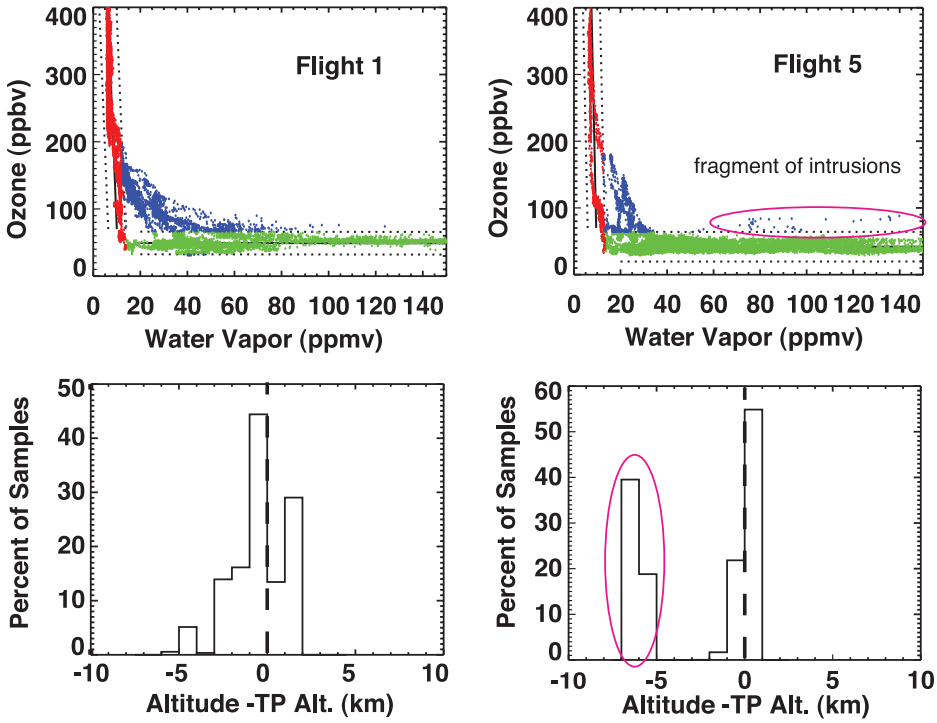

Figure 7. (top) Stratospheric branch (red), tropospheric branch (green) and the mixed air mass (blue) defined using linear regressions to the observed O_3-H_2O correlation for both flights. The black solid and dash lines mark the fit and the 3σ distribution of the fit, respectively. (bottom) Histograms showing the distribution of the mixed samples (blue points) in altitude relative to the thermal tropopause (1 km bins). The pink ovals mark the air mass that was sampled ~4–5 km altitude range during take off and is identified as a fragment of stratospheric intrusion. See Figure 5. The thermal tropopause heights are based on the GFS analyses. The uncertainty of the heights compared to the heights from aircraft temperature profiles are discussed in the text.

[28] It is readily apparent from the corner of the L that the chemical transition sampled by this flight has two different regimes, marked by the two distinct groups of points, one connects the stratospheric and tropospheric branches along curved mixing lines and the other approximately forms the corner of the L. These two regimes can be identified as chemical transitions with and without significant mixing, respectively, and will be further discussed in the next section. The transition between the green and red points in Figure 6 (top) indicates that the thermal tropopause is located in the tracer space roughly around the corner of "L" in the region without significant mixing, and spans the entire range of the mixing region where mixing is extensive.

[29] The air mass between the thermal and dynamical tropopause, highlighted in blue in Figure 6 (bottom), spans the entire mixing region in the tracer space and has almost no overlap with the stratospheric branch, but does have extensive overlap with the tropospheric branch. In other words, in tracer space, the air mass between the thermal and PV tropopause appears to be a mixture of stratospheric and tropospheric air, but predominantly of tropospheric character. Since a significant fraction of the mixed air parcels lie in the layer between the two definitions of the tropopause, this result also explains the difference in the location of the chemical transition layer identified using PV and thermal definitions of the tropopause [*Fischer et al.*, 2000; *Hoor et al.*, 2002, 2004; *Pan et al.*, 2004, 2007]. That is, the mixing region is often above the 2 pvu surface, and using that surface to define the tropopause would classify the mixed air as part of the stratosphere.

[30] Figure 6 provides a perspective that the choice of tropopause definition may result in different views of how STE alters the chemical composition of the UTLS region. Using the thermal definition, the flight 1 results show that the mixing across the tropopause enhanced the CO value in the lower stratosphere (indicated by the red mixing lines in Figure 6) and also enhance the ozone value in the upper troposphere (indicated by the green mixing lines in the Figure 6). Using the 2 pvu definition, the mixing mainly influence the air mass above the tropopause, because, by this definition, most of the mixed parcels (blue points in Figure 6) are above the tropopause. To go beyond the subjective choice of whether the mixing layer is a part of the stratosphere or partly within the troposphere depending on the choice of reference level, we present a diagnostic, in section 3.3, to characterize the depth of air mass that is influenced by mixing, and a trajectory analysis, in section 3.4, to examine the transport origins and fate of these air parcels.

3.3. Mixing Diagnoses

[31] As shown in the previous section, neither the thermal nor the dynamical tropopause can serve to isolate effectively the stratosphere from the troposphere in the tracer-tracer

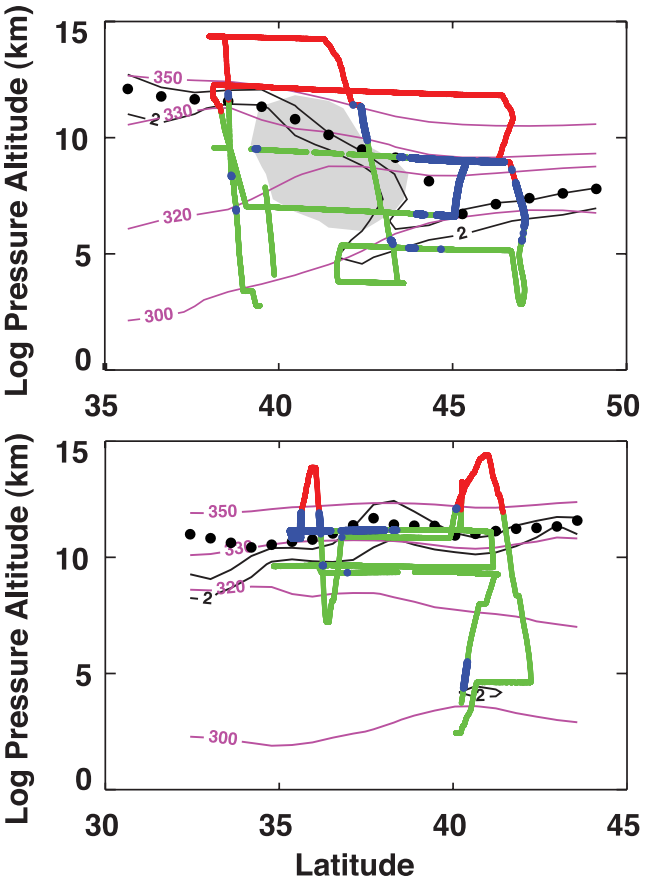

Figure 8. Air mass identification based on tracer correlation analyses, shown in Figure 7, mapped to the flight track. The stratospheric, tropospheric and mixed air masses are shown in red, green, and blue, respectively. The dynamical background of the flights is shown by PV (black contours), isentropes (purple contours), the thermal tropopause (black dots) and the zonal wind field (50 m/s, gray shade), all based on the GFS data. Note that the GFS data are 1800 UT analyses and the in situ measurements on GV are asynoptic and took place over ~8-hour durations. The display of the background relative to the GV track is therefore an approximation.

space where extensive mixing is present. In this section, we focus on the mixed air parcels, and examine where they are observed, as well as the distribution of these measurements in the flight cross section and relative to the thermal and dynamical tropopause.

[32] Following the method described by *Pan et al.* [2004, 2007], the observed air parcels can be categorized empirically as stratospheric, tropospheric, or mixed, on the basis of their locations in the O_3-H_2O tracer space. This analysis for flights 1 and 5 is shown in Figure 7 (top). Here the identification of the stratospheric branch is made by a linear fit to data points with $H_2O < 12$ ppmv. The tropospheric branch is identified by a linear fit to data points with $O_3 < 65$ ppbv. The data points within 3σ of the fit are categorized as stratospheric (red) or tropospheric (green). The data points outside the 3σ of the both branches are considered mixed (blue). These critical values are somewhat arbitrary. The variation of them will change the detail but not the overall characteristics of the resulting mixed region. In comparison, the mixed region in flight 1 is more extensive than flight 5.

[33] The second part of Figure 7 (bottom) shows the distributions of the mixed parcels in z_r (altitude relative to the thermal tropopause). In the case of flight 1, the mixed parcels are found in a range approximately −3 to +2 km around the thermal tropopause. In other words, there is a mixing layer with a depth of ~5 km. For flight 5, on the other hand, mixed parcels are found to be within roughly ±1 km of the thermal tropopause. There is also a group of mixed air parcels found ~5 km below the tropopause. These parcels were observed during the initial ascent after takeoff when the aircraft passed through a fragment of stratospheric intrusion, as indicated by high PV (40° and in the 4–5 km altitude range, shown in Figure 5, also see Figure 8). These parcels correspond to the scattered blue points above the tropospheric branch in Figure 7 (top right). It is important to note that in both cases the thermal tropopause approximately marks the center of the mixing layer. The contrast between the two flights further indicates that the larger depth of the mixing layer occurs near the jet stream, where turbulence due to shear instability and wave breaking often occurs [e.g., *Danielsen*, 1968; *Cho et al.*, 1999; *Haynes and Shuckburgh*, 2000; *Scott and Cammas*, 2002].

[34] Figure 8 displays the distributions of these three categories of air parcels along the flight tracks, together with the cross section of dynamical variables from the 1800 UT analyses (which is an approximation to the flight cross section, as explained before). It is readily apparent from Figure 8 that significantly more mixed air was observed on flight 1 than on flight 5. On flight 1, mixed parcels were preferentially observed on the cyclonic side of the jet, where the thermal tropopause is weakly defined. The mixing on flight 5 and the anticyclonic side of the jet on flight 1 is at a minimum. This result shows that if the ExTP is treated as a layer, or ExTL, this layer is spatially inhomogeneous. Mixing occurs prevalently on the cyclonic (poleward) side of the jet, creating a less abrupt chemical transition between the stratosphere and troposphere and is consistent with the profile analyses in section 3.1. The fact that the PV tropopause and the thermal tropopause separate significantly in this region can be viewed as an indication of a less distinct tropopause. Mixing brings high ozone mixing ratios to the layer below the thermal tropopause (also indicated in Figure 4), which could explain the previously observed lower ozone tropopause in the region of indefinite thermal tropopause [*Bethan et al.*, 1996].

[35] Note that it is difficult to pinpoint when and where mixing occurred using these observations alone, as the mixed parcels are the cumulative effect of mixing that could have occurred locally or upstream during previous mixing events.

3.4. Trajectory Analyses

[36] Trajectory calculations are used to examine the origins and the fate of the air mass in the region of the intrusion observed during flight 1. The primary motivation for the analyses is to see whether the air mass in the intrusion, i.e., between the thermal and dynamical tropopause, subsequently entered the troposphere irreversibly.

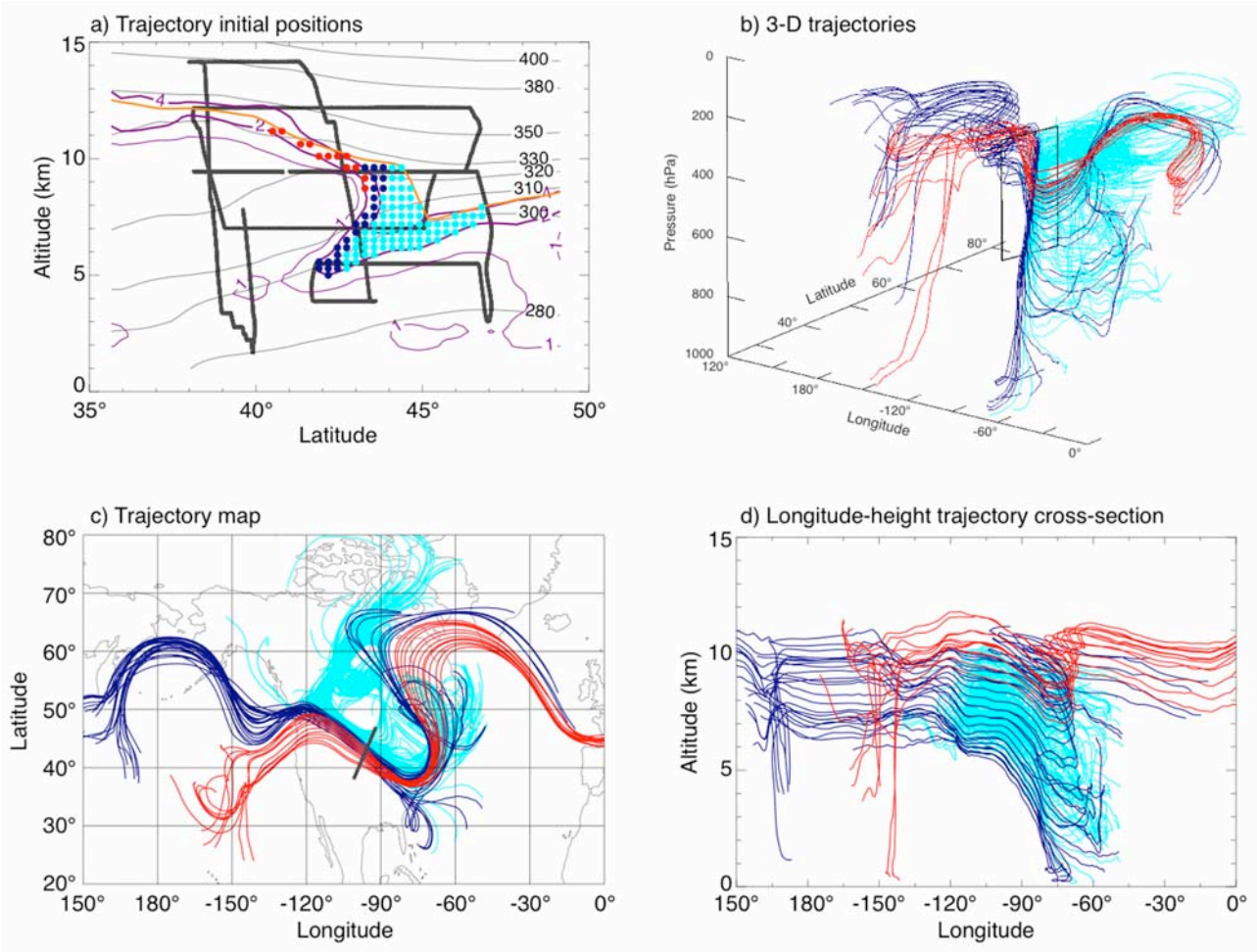

Figure 9. (a) Initial locations and (b–d) 3-day forward and backward trajectories for air parcels initialized along a cross section through the jet at 1800 UT on 1 December. In Figure 9a the potential temperature (black), PV (purple), and tropopause height (orange) are from the 1800 UT GFS analysis. The gray line is the aircraft flight track projected onto the cross section. The location of the cross section is also marked on the map projection (Figure 9c) by the gray line. Parcels are color coded by their upstream region of origin: dark blue, main jet; light blue, high latitudes; red, subtropics. See text for more details.

The calculations used a 3-D trajectory model (TRAJ3D), based on *Bowman* [1993], driven by NCEP GFS wind fields. Trajectories are calculated kinematically in pressure coordinates using three-dimensional winds (u, v, ω) from the 6-hourly NCEP GFS operational analysis.

[37] Figure 9 shows forward and backward three-dimensional 3-day trajectories for air parcels in a cross section through the intrusion. Figure 9a shows the initial locations of the parcels, which were initialized on 1800 UT 1 December along an approximately southwest to northeast cross section through the fold. The location of the cross section is marked by the black line in Figure 9c (the map view of the trajectories), where the backward trajectories (west of the line) and the forward trajectories (east of the line) connect. The cross section, also indicated by the black box in the 3-D view (Figure 9b), approximately coincides with the aircraft flight track. The potential temperature, PV, and tropopause height in Figure 9a are from the 1800 UT GFS analysis on 1 December. The parcels plotted in Figure 9 lie on the cross section and are restricted to the area between 40° and 47°N latitude and between the thermal tropopause (orange line) and the 2 pvu surface (heavy purple line). The shape of the intrusion is apparent in the deformation and folding of the PV surface.

[38] Parcels are classified and color-coded subjectively by their upstream regions of origin, which can be seen most clearly in Figure 9c. Within the preceding 3 days, parcels colored dark blue moved primarily across the Pacific following the polar jet. Parcels colored light blue came from the high-latitude branch of the jet (the Arctic jet) and merged into the polar jet stream approximately 1 day before the time of the cross section. Parcels colored red came primarily from the subtropics, indicating the influence of the subtropical jet at a higher altitude. Some red parcels ascended from near the surface in warm conveyor belts [e.g., *Stohl and Trickl*, 1999] associated with synoptic-scale systems over the Pacific. These parcels traveled in the jet just below the thermal tropopause.

[39] Figures 9b and 9d show three-dimensional and longitude-altitude views of the trajectories, respectively. The upstream ascent of some red and dark blue parcels into the upper troposphere can be seen in these panels. The forward trajectories, which are downstream and east of the location of the cross section, show that many of the light and dark blue parcels from the intrusion descended into the middle and lower troposphere, while the red parcels and some dark blue parcels remained in the jet and moved rapidly across the Atlantic. By 4 December, 3 days after arriving in the fold, the PV for significant fraction (~50%) of the parcels becomes less than 2 pvu. This is a strong indication of the irreversibility of the intrusion.

[40] It is important to note that as the trajectories converge, air from different origins would have likely mixed. The chemical composition of the parcels along their paths would change. The colors of the trajectories, therefore, do not indicate that the parcels remain unmixed as their trajectories diverge downstream. A more detailed study of mixing would require models more sophisticated than simple trajectory calculations [e.g., *McKenna et al.*, 2002; *Pan et al.*, 2006; *Konopka et al.*, 2006].

4. Conclusions and Discussions

[41] We have presented an analysis of in situ measurements of ozone and water vapor on two HIAPER flights during December 2005. Using these observations and large-scale meteorological analyses, we address the problem of characterizing the transport boundary between the stratosphere and troposphere. The results of our observations and analyses lead to the following conclusions.

[42] The sharpness of the chemical transition across the ExTP, observed during the START experiment, correlates with the sharpness of static stability change in the tropopause region. Abrupt chemical transitions were observed both on flight 5, sampled in a region away from the jet stream, and at the anticyclonic (equatorward) side of the jet on flight 1. Mixing near the tropopause was found to be minimal in these regions of sharp thermal tropopause. In other words, the thermal tropopause in these locations appears to behave as a transport barrier to some degree, and it marks the boundary of chemically distinct stratospheric and tropospheric air masses.

[43] A much more gradual chemical transition was observed on the cyclonic (poleward) side of the jet during flight 1, associated with a less definite thermal tropopause, as indicated by the much weaker static stability gradient across the tropopause (Figure 5), and a significant separation of the thermal and dynamical tropopause (represented by 2 pvu surface). An extensive layer (~5 km) of mixed stratospheric and tropospheric air, identified by the tracer correlation between O_3 and H_2O vapor, was found in this region.

[44] These observations suggest that, if the ExTP is treated as a transition layer, the thickness of the layer appears to have strong spatial variation. The jet location where an extensive mixing layer was observed on flight 1 is known as the preferred location of STE from both observations and model studies [e.g., *Shapiro*, 1980; *Wernli and Bourqui*, 2002; *Stohl et al.*, 2003]. The layer of mixed air indicates the impact of active two-way exchange on the distribution of chemical tracers. Since neither the thermal nor the dynamical tropopause simply separate the stratospheric and tropospheric air masses in this region, the difference of the two definitions here may be viewed as an indication that the tropopause as a transport barrier exists to a much lesser degree under these conditions.

[45] Stratosphere-to-troposphere transport in the region of cyclonic flow has been discussed in detail previously by *Price and Vaughan* [1993], with emphasis on midlatitude cutoff lows. Various PV nonconservative processes, including convective erosion, turbulent mixing and radiative heating/cooling are considered necessary for the irreversible exchange to occur. The presence of the mixed parcels from our analyses here is evidence of irreversible exchange and the presence of turbulent mixing, likely associated with the wind shear of the jet stream. Our analyses also suggest that the previously observed lower ozone tropopause in the cyclonic region [*Bethan et al.*, 1996] may be a result of mixing.

[46] We chose 2 pvu as the dynamical tropopause in this study, because it has been the most popular choice of dynamical definition in STE studies. Our results, however, indicate that using this surface as the transport boundary will tend to under estimate the influence of STE to the upper troposphere. The tracer correlation analysis, shown in Figure 6, indicates that the air mass between the thermal tropopause and 2 pvu is largely of tropospheric chemical characteristics. Furthermore, the ozone–PV correlations given in Figure 4 indicate that stratospheric ozone values correlates with air mass of 4 pvu or greater.

[47] These conclusions are based on a small number of aircraft flights and limited trace species measurements and as such need to be investigated further in future field missions. For this application the use of tracers of different chemical lifetimes would be extremely valuable.

[48] We note that the ozone mixing ratio measured within the fold during flight 1 is relatively low, mostly 100 ppbv or lower (Figures 3 and 4). This is well correlated with the relatively low ozone concentration in the lowermost stratosphere during the month of the START experiment. This is consistent with the known seasonal cycle of lowermost stratospheric ozone. Observations from satellite, ozonesondes, and aircraft all indicate that the maximum is in Spring and the minimum is in Autumn [e.g., *Pan et al.*, 1997; *Logan*, 1999; *Krebsbach et al.*, 2006]. The low ozone observation made on flight 1 reflects the near minimum in the seasonal cycle. In a future experiment we plan to verify that ozone transport in tropopause folding events is more efficient in the Spring season when lower stratospheric ozone levels are higher.

[49] **Acknowledgments.** This work is supported in part by the National Science Foundation through its support to the University Corporation for Atmospheric Research (UCAR) and in part supported by the National Science Foundation under grant 0605739. The authors thank NCAR research aviation facility staff for their dedicated effort operating HIAPER. In particular, we thank J. Jensen and A. Schanot for managing the ProgSci project; W. Cooper for help with flight planning; R. Ruth for data archive and support; and HIAPER pilots H. Boynton, R. Maxson, L. Genzlinger, and E. Ringleman for piloting the research flights.

References

Bethan, S., G. Vaughan, and S. J. Reid (1996), A comparison of ozone and thermal tropopause heights and the impact of tropopause definition on

quantifying the ozone content of the troposphere, *Q. J. R. Meteorol. Soc.*, *122*, 929–944.

Bian, J., A. Gettelman, H. Chen, and L. L. Pan (2007), Validation of satellite ozone profile retrievals using Beijing ozonesonde data, *J. Geophys. Res.*, *112*, D06305, doi:10.1029/2006JD007502.

Bowman, K. P. (1993), Large-scale isentropic mixing properties of the Antarctic polar vortex from analyzed winds, *J. Geophys. Res.*, *98*, 23,013–23,027.

Bowman, K. P., L. L. Pan, T. Campos, and R. Gao (2007), Observations of fine-scale transport structure in the upper troposphere from HIAPER, *J. Geophys. Res.*, *112*, D18111, doi:10.1029/2007JD008685.

Cho, J. Y. N., et al. (1999), Observations of convective and dynamical instabilities in tropopause folds and their contribution to stratosphere-troposphere exchange, *J. Geophys. Res.*, *104*, 21,549–21,568.

Cooper, O., et al. (2004), On the life cycle of a stratospheric intrusion and its dispersion into polluted warm conveyor belts, *J. Geophys. Res.*, *109*, D23S09, doi:10.1029/2003JD004006.

Danielsen, E. F. (1968), Stratospheric-tropospheric exchange based on radioactivity, ozone and potential vorticity, *J. Atmos. Sci.*, *25*, 502–518.

Dessler, A. E., E. J. Hintsa, E. M. Weinstock, J. G. Anderson, and K. R. Chan (1995), Mechanisms controlling water vapor in the lower stratosphere: "A tale of two stratospheres," *J. Geophys. Res.*, *100*(D11), 23,167–23,172.

Fetzer, E. J., B. H. Lambrigtsen, A. Eldering, H. H. Aumann, and M. T. Chahine (2006), Biases in total precipitable water vapor climatologies from Atmospheric Infrared Sounder and Advanced Microwave Scanning Radiometer, *J. Geophys. Res.*, *111*, D09S16, doi:10.1029/2005JD006598.

Fischer, H., F. G. Wienhold, P. Hoor, O. Bujok, C. Schiller, P. Siegmund, M. Ambaum, H. A. Scheeren, and J. Lelieveld (2000), Tracer correlations in the northern high latitude lowermost stratosphere: Influence of cross-tropopause mass exchange, *Geophys. Res. Lett.*, *27*, 97–100.

Haynes, P., and E. Shuckburgh (2000), Effective diffusivity as a diagnostic of atmospheric transport: 1. Stratosphere, *J. Geophys. Res.*, *105*(D18), 22,777–22,794.

Hegglin, M. I., D. Brunner, T. Peter, P. Hoor, H. Fischer, J. Staehelin, M. Krebsbach, C. Schiller, U. Parchatka, and U. Weers (2006), Measurements of NO, NOy, N_2O, and O_3 during SPURT: Seasonal distributions and correlations in the lowermost stratosphere, *Atmos. Chem. Phys.*, *6*, 1331–1350.

Highwood, E. J., and B. J. Hoskins (1998), The tropical tropopause, *Q. J. R. Meteorol. Soc.*, *124*, 1579–1604.

Hintsa, E. J., et al. (1998), Troposphere-to-stratosphere transport in the lowermost stratosphere from measurements of HO, CO_2, N_2O and O_3, *Geophys. Res. Lett.*, *25*(14), 2655–2658.

Hoerling, M. P., T. K. Schaack, and A. J. Lenzen (1991), Global objective tropopause analysis, *Mon. Weather Rev.*, *119*, 1816–1831.

Hoinka, K.-P. (1997), The tropopause: Discovery, definition and demarcation, *Meteorol. Z.*, *6*, 281–303.

Holton, J. R., P. H. Haynes, M. E. McIntyre, A. R. Douglass, R. B. Rood, and L. Pfister (1995), Stratosphere-troposphere exchange, *Rev. Geophys.*, *33*, 403–439.

Hoor, P., H. Fischer, L. Lange, J. Lelieveld, and D. Brunner (2002), Seasonal variations of a mixing layer in the lowermost stratosphere as identified by the CO-O_3 correlation from in situ measurements, *J. Geophys. Res.*, *107*(D5), 4044, doi:10.1029/2000JD000289.

Hoor, P., C. Gurk, D. Brunner, M. I. Hegglin, H. Wernli, and H. Fischer (2004), Seasonality and extent of extratropical TST derived from in-situ CO measurements during SPURT, *Atmos. Chem. Phys.*, *4*, 1427–1442.

Hoskins, B. J. (1991), Towards a PV-θ view of the general circulation, *Tellus, Ser. A B*, *43*, 27–35.

Hoskins, B. J., M. E. McIntyre, and A. W. Robertson (1985), On the use and significance of isentropic potential vorticity maps, *Q. J. R. Meteorol. Soc.*, *111*, 877–946.

Karpechko, A., A. Lukyanov, E. Kyro, S. Khaikin, L. Korshunov, R. Kivi, and H. Vomel (2007), The water vapour distribution in the Arctic lowermost stratosphere during the LAUTLOS campaign and related transport processes including stratosphere-troposphere exchange, *Atmos. Chem. Phys.*, *7*, 107–119.

Kochanski, A. (1955), Cross sections of the mean zonal flow and temperature along 80 degrees W, *J. Meteorol.*, *12*, 95–106.

Konopka, P., et al. (2006), Contribution of mixing to the upward transport across the TTL, *Atmos. Chem. Phys. Disc.*, *6*, 12,217–12,266.

Krebsbach, M., et al. (2006), Seasonal cycles and variability of O_3 and H_2O in the UT/LMS during SPURT, *Atmos. Chem. Phys.*, *6*, 109–125.

Law, K., L. Pan, H. Wernli, H. Fischer, P. Haynes, R. Salawitch, B. Karcher, M. Prather, S. Doherty, and A. R. Ravi (2005), Processes governing the chemical distribution of the extra-tropical UTLS, *IGAC Newsl.*, *32*, 2–22.

Logan, J. A. (1999), An analysis of ozonesonde data for the troposphere: Recommendations for testing 3-D models and development of a gridded climatology for tropospheric ozone, *J. Geophys. Res.*, *104*, 16115–16149.

Marcy, T., et al. (2004), Quantifying stratospheric ozone in the upper troposphere with in situ measurements of HCl, *Science*, *304*, 261–265.

McKenna, D. S., P. Konopka, J. Grooß, G. Günther, R. Müller, R. Spang, D. Offermann, and Y. Orsolini (2002), A new Chemical Lagrangian Model of the Stratosphere (CLaMS): 1. Formulation of advection and mixing, *J. Geophys. Res.*, *107*(D16), 4309, doi:10.1029/2000JD000114.

Monahan, K. P., L. L. Pan, A. McDonald, G. E. Bodeker, J. C. Wei, S. George, C. Barnet, and E. S. Maddy (2007), Validation of AIRS v4 ozone profiles in the UTLS using ozonesondes from Lauder, NZ and Boulder, USA, *J. Geophys. Res.*, *112*, D17304, doi:10.1029/2006JD008181.

Palmén, E., and C. W. Newton (1969), *Atmospheric Circulation Systems*, Elsevier, New York.

Pan, L., S. Solomon, W. Randel, J.-F. Lamarque, P. Hess, J. Gille, E.-W. Chiou, and M. P. McCormick (1997), Hemispheric asymmetries and seasonal variations of the lowermost stratospheric water vapor and ozone derived from SAGE II data, *J. Geophys. Res.*, *102*(D23), 28,177–28,184.

Pan, L. L., W. J. Randel, B. L. Gary, M. J. Mahoney, and E. J. Hintsa (2004), Definitions and sharpness of the extratropical tropopause: A trace gas perspective, *J. Geophys. Res.*, *109*, D23103, doi:10.1029/2004JD004982.

Pan, L. L., P. Konopka, and E. V. Browell (2006), Observations and model simulations of mixing near the extratropical tropopause, *J. Geophys. Res.*, *111*, D05106, doi:10.1029/2005JD006480.

Pan, L. L., J. C. Wei, D. E. Kinnison, R. R. Garcia, D. J. Wuebbles, and G. P. Brasseur (2007), A set of diagnostics for evaluating chemistry-climate models in the extratropical tropopause region, *J. Geophys. Res.*, *112*, D09316, doi:10.1029/2006JD007792.

Patmore, N., and R. Toumi (2006), An entropy-based measure of mixing at the tropopause, *Q. J. R. Meteorol. Soc.*, *132*, 1949–1967.

Price, J. D., and G. Vaughan (1993), The potential for stratosphere-troposphere exchange in cut-off-low systems, *Q. J. R. Meteorol. Soc.*, *119*, 343–365.

Proffitt, M. H., and R. J. McLaughlin (1983), Fast-response dual beam UV-absorption ozone photometer suitable for use on stratospheric balloons, *Rev. Sci. Instrum.*, *54*, 1719–1728.

Randel, W. J., D. J. Seidel, and L. L. Pan (2007), Observational characteristics of double tropopauses, *J. Geophys. Res.*, *112*, D07309, doi:10.1029/2006JD007904.

Ray, E. A., F. L. Moore, J. W. Elkins, G. S. Dutton, D. W. Fahey, H. Vömel, S. J. Oltmans, and K. H. Rosenlof (1999), Transport into the Northern Hemisphere lowermost stratosphere revealed by in situ tracer measurements, *J. Geophys. Res.*, *104*(D21), 26,565–26,580.

Ridley, B. A., et al. (2004), Convective transport of reactive constituents to the tropical and mid-latitude tropopause region: I. Observations, *Atmos. Environ.*, *38*, 1259–1274.

Scott, R. K., and J.-P. Cammas (2002), Wave breaking and mixing at the subtropical tropopause, *J. Atmos. Sci.*, *59*, 2347–2361.

Shapiro, M. A. (1980), Turbulent mixing within tropopause folds as a mechanism for the exchange of chemical constituents between the stratosphere and troposphere, *J. Atmos. Sci.*, *37*, 994–1004.

Sherwood, S. C., and A. E. Dessler (2000), On the control of stratospheric humidity, *Geophys. Res. Lett.*, *27*(16), 2513–2516.

Stohl, A., and T. Trickl (1999), A textbook example of long-range transport: Simultaneous observation of ozone maxima of stratospheric and North American origin in the free troposphere over Europe, *J. Geophys. Res.*, *104*, 30,445–30,462.

Stohl, A., H. Wernli, P. James, M. Bourqui, C. Forster, M. A. Liniger, P. Seibert, and M. Sprenger (2003), A new perspective of stratosphere–troposphere exchange, *Bull. Am. Meteorol. Soc.*, *84*, 1565–1573.

Susskind, J., C. Barnet, J. Blaisdell, L. Iredell, F. Keita, L. Kouvaris, G. Molnar, and M. Chahine (2006), Accuracy of geophysical parameters derived from Atmospheric Infrared Sounder/Advanced Microwave Sounding Unit as a function of fractional cloud cover, *J. Geophys. Res.*, *111*, D09S17, doi:10.1029/2005JD006272.

Wernli, H., and M. Bourqui (2002), A Lagrangian "1-year climatology" of (deep) cross-tropopause exchange in the extratropical Northern Hemisphere, *J. Geophys. Res.*, *107*(D2), 4021, doi:10.1029/2001JD000812.

Wirth, V. (2001), Cyclone-anticyclone asymmetry concerning the height of the thermal and the dynamical tropopause, *J. Atmos. Sci.*, *58*, 26–37.

World Meteorological Organization (1957), Meteorology—A three-dimensional science: Second session of the Commission for Aerology, *WMO Bull.*, *4*(4), 134–138.

World Meteorological Organization (2002), Scientific assessment of ozone depletion: 2002, *WMO Global Ozone Res. Monit. Proj. Rep. 47*, 498 pp., World Meteorol. Org., Geneva, Switzerland. (Available at http://ozone.unep.org/Publications/6v_science%20assess%20panel.shtml)

Young, L.-H., et al. (2007), Enhanced new particle formation observed in the northern midlatitude tropopause region, *J. Geophys. Res.*, *112*, D10218, doi:10.1029/2006JD008109.

Zahn, A., and C. A. M. Brenninkmeijer (2003), New directions: A chemical tropopause defined, *Atmos. Environ.*, *37*, 439–440.

Zahn, A., et al. (2000), Identification of extratropical two-way troposphere-stratosphere mixing based on CARIBIC measurements of O_3, CO, and ultrafine particles, *J. Geophys. Res.*, *105*, 1527–1535.

C. Barnet, National Environmental Satellite Data and Information Service, NOAA, Camp Springs, MD 20746, USA.

K. P. Bowman, Department of Atmospheric Sciences, Texas A&M University, College Station, TX 77843-3150, USA.

T. Campos, C. Davis, L. L. Pan, W. J. Randel, B. A. Ridley, S. Schauffler, and M. Shapiro, National Center for Atmospheric Research, Boulder, CO 80307-3000, USA. (liwen@ucar.edu)

R. S. Gao, Chemical Sciences Division, Earth System Research Laboratory, NOAA, Boulder, CO 80305, USA.

J. C. Wei, QSS Group, Inc., Lanham, MD 20706, USA.